

Principal Component Analysis (PCA) to transform the system of correlated coordinates into a system of uncorrelated coordinates ordered by principal components of decreasing variance (Steiner et al. 2009). Nevertheless, in some cases the ‘traditional’ line-profile fitting method must be additionally used to properly extract the flux distribution and kinematics of the emitting gas.

In this work I present an automated line-PROFILE FITTING routine (PROFIT) to be used to extract the gaseous kinematics and flux distribution from fits data cubes. This routine is written in IDL¹ language and allows the fit of the observed profiles by Gauss-Hermite series or Gaussian curves. The fit of Gauss-Hermite series has been chosen because it preserve the velocity information of the emitting gas by the fitting of the wing of the emission-line profiles. Such information could be lost in the fit of a single Gaussian curve for an asymmetric emission-line profile. Another advantage of the Gauss-Hermite profile is that it can be easily be implemented in an automated routine than multiple Gaussian fit – which would also preserve the velocity information.

The paper is organized as follows. In Section 2 I present the formalism of the Gauss-Hermite and Gaussian functions; Sec. 3 presents the PROFIT routine and in Sec. 4 I discuss an application of the routine for the Seyfert galaxy Mrk1066. Sec. 5 presents the final remarks of the present work.

2 Gauss-Hermite *versus* Gaussian

The Gauss-Hermite series can be written as (e.g. van der Marel & Franx 1993; Gerhard 1993; Cappellari & Emswiler 2004):

$$GH = \frac{A\alpha(w)}{\sigma} \sum_{j=0}^n h_j H_j(w) \quad (1)$$

where

$$w \equiv \frac{\lambda - \lambda_c}{\sigma} \quad (2)$$

and

$$\alpha(w) = \frac{1}{\sqrt{2\pi}} e^{-w^2/2}, \quad (3)$$

A is the amplitude of the Gauss-Hermite series, λ_c is the peak wavelength, h_j are the Gauss-Hermite moments and $H_j(w)$ are the Hermite polynomials.

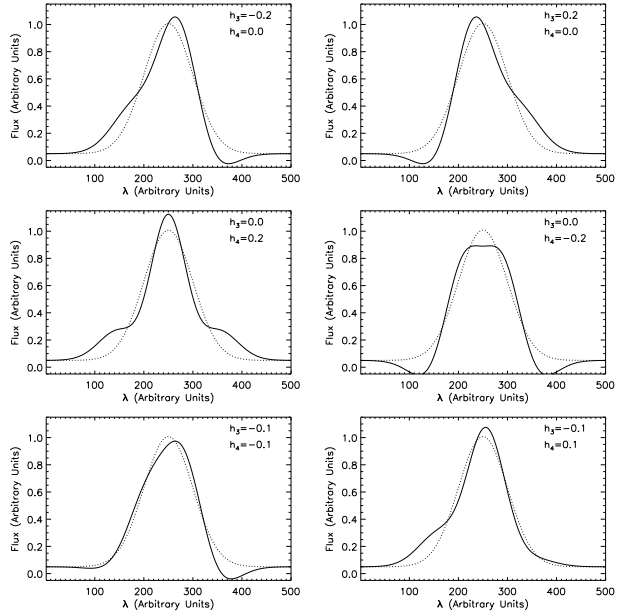


Fig. 1 Comparison of Gaussian curves (dotted lines) with Gauss-Hermite series (continuous lines) for the h_3 and h_4 values shown at the top-left corner of each panel. The amplitude, central wavelength and σ are the same for both functions and have arbitrary values.

If the emission-line profile is similar to a Gaussian we can truncate the sum on $n = 4$ and assume $h_0 = H_0(w) = 1$, $h_1 = h_2 = 0$ (van der Marel & Franx 1993). This is a good approximation if the emission-line presents an asymmetric profile, such as the blue or red wings frequently observed for the line emission from ionized gas in the narrow line region of active galaxies (Riffel, Storchi-Bergmann & Nagar 2010; Riffel et al. 2009a; Komossa et al. 2008). Using the approximation above, the Eq. 1 can be written as

$$GH = \frac{A\alpha(w)}{\sigma} [1 + h_3 H_3(w) + h_4 H_4(w)], \quad (4)$$

where

$$H_3(w) = \frac{1}{\sqrt{6}} (2\sqrt{2}w^3 - 3\sqrt{2}w) \quad (5)$$

and

$$H_4(w) = \frac{1}{\sqrt{24}} (4w^4 - 12w^2 + 3). \quad (6)$$

The h_3 Gauss-Hermite moment measures asymmetric deviation from a Gaussian profile, such as blue or red wings, while the h_4 moment quantify the peakedness of the profile, with $h_4 > 0$ for a more peaked and $h_4 < 0$ for a broader profile than a Gaussian

¹<http://www.ittvis.com/>

curve. A particular case of Eq. 4 is $h_3 = h_4 = 0$, when it becomes a Gaussian curve. In Figure 1, I present a sample of profiles for Gauss-Hermite series with distinct h_3 and h_4 values (continuous lines) and Gaussian curves (dotted lines). The amplitude, central wavelength and σ are the same for Gaussian and Gauss-Hermite functions and have arbitrary values. The h_3 and h_4 moments are shown at the top-left corner of each panel and have values typically observed for the narrow line region of active galaxies (e.g. Riffel & Storchi-Bergmann 2010). The comparison of observed emission-line profiles, such as those of Mrk 1066 from Riffel, Storchi-Bergmann & Nagar (2010) (see Sec. 4), with the profiles shown in Figure 1 suggests that the observations are better reproduced by Gauss-Hermite series than by Gaussian curves in most cases.

3 The PROFIT routine

The model of each emission-line profile is constructed by the sum of Eq. 4 with a linear equation, in order to represent the underlying continuum emission. The resulting equation contains seven free parameters ($A, \lambda_c, \sigma, h_3, h_4$ plus two parameters for the linear equation), which can be determined by fitting the line profiles. In case of Gaussian fitting the h_3 and h_4 are fixed at zero and thus the remaining 5 parameters may be obtained from the fit of the observed profile. These parameters can be obtained by solving a Least-squares problem.

The PROFIT routine was written in IDL language and performs the fit of the observed profile using the MPFIT² routine, which is the MINPACK1 implementation (Moré, Garbow & Hillstom 1980) of the Levenberg-Marquardt method for nonlinear least-squares problems. The IDL language was chosen because it is extensively used in astronomy and allows read the data cube from standard fits format to an array using the NASA-Goddard Space Flight Center IDL Astronomy User's Library³. The algorithm recovers the emission-line flux distribution and kinematics as follows:

- 1- Initial guesses for the centroid wavelength and velocity dispersion are given by the user. The initial guesses for h_3 and h_4 are fixed at zero;
- 2- The input data cube in standard fits format (in which the spatial dimensions are in the x and y-axis and spectral pixels are in the z-axis) is converted into an array.

Next steps are done individually for each spectrum:

- 3- Calculates the spectral region to be fitted using the initial guess for the centroid wavelength and the spectral information (spectral sampling and initial wavelength) contained in the header of the data cube fits file.
- 4- Normalizes the spectrum by its maximum value and obtain initial guesses for the parameters of the linear equation and amplitude of the Gauss-Hermite series (or Gaussian);
- 5- Performs the nonlinear least-squares fitting of the observed profile by the adopted the model using the Levenberg-Marquardt method;
- 6- Writes the solution to the output file;
- 7- If χ^2 is less than a maximum value (defined by the user) the fitted parameters are used as initial guesses for the fit of the next spectrum. Otherwise uses the initial guesses of item 1;
- 8- Repeats items 3–8 for all spectra.
- 9- Writes the solutions to a Multiple Extensions FITS (MEF) file. The output MEF file will contain 7 extensions containing the: [0] emission-line flux distribution; [1] centroid velocity field; [2] velocity dispersion map; [3] h_3 map; [4] h_4 map; [5] reduced χ^2 map defined as

$$\chi^2 = \sum_p \frac{(O_p - M_p)^2}{\sigma_O^2} \frac{1}{(N - N_{\text{par}})}, \quad (7)$$

where O_p is the observed spectra, M_p is the best fit model, σ_O^2 is the variance of the observed spectra, N is the number of spectral pixels (p) used in the fit and N_{par} is the number of free parameters; and [6] flux distribution obtained directly by integration the emission line profile and subtracting a continuum obtained by the average of continuum regions at both sides of the line profile.

4 A First Application

In Fig. 2 I present an example of the use of PROFIT to fit the emission-line profile of [FeII] at $\lambda = 1.257 \mu\text{m}$ at $1''$ north-west of the nucleus of the Seyfert galaxy Mrk 1066. This spectrum was extracted from Gemini's Near-infrared Integral Field Spectrograph (NIFS) observations (program ID: GN-2008A-Q-30) within an aperture of $0.3 \times 0.3 \text{ arcsec}^2$ (see Riffel, Storchi-Bergmann & Nagar (2010) for a description of the observations and data reduction procedures). The observed profile is shown as a continuous line, the fitting of Gauss-Hermite series as a dashed line, the fitting of a single Gaussian as a dot-dashed line and the two Gaussian curves fit as a dotted line. The best Gauss-Hermite fit is obtained

²The MPFIT routine can be obtained from the Markwardt IDL Library at <http://cow.physics.wisc.edu/~craigm/idl/idl.html>

³The IDL Astronomy User's Library can be obtained from <http://idlastro.gsfc.nasa.gov>

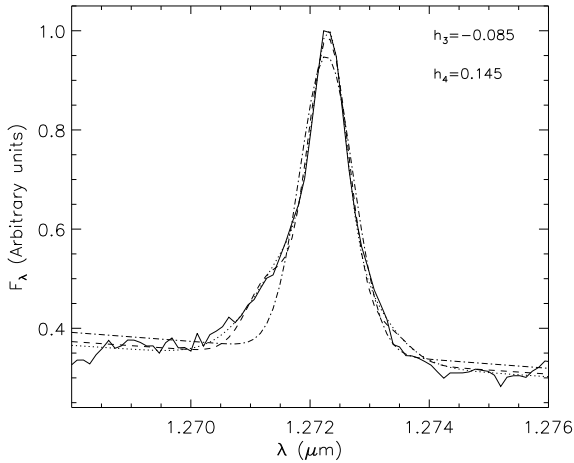


Fig. 2 Example of fitting using PROFIT routine for the [Fe II] $\lambda 1.2570 \mu\text{m}$ emission-line profile for a spectrum extracted within an aperture of $0.3 \times 0.3 \text{ arcsec}^2$ at 1 arcsec north-west of the nucleus of Mrk 1066. The continuous line represents the observed profile, the dashed line the resulting Gauss-Hermite fit, the dot-dashed line the fit of a single Gaussian and the dotted line the resulting fit by two Gaussian curves.

for a central wavelength $\lambda_c = 12722.6 \pm 0.2 \text{ \AA}$, a velocity dispersion of $\sigma = 114.3 \pm 8.8 \text{ km s}^{-2}$ and higher order Gauss-Hermite moments $h_3 = -0.085 \pm 0.017$ and $h_4 = 0.145 \pm 0.014$ and resulted in a $\chi^2 = 0.014$. The best fit obtained using a Gaussian curve has $\chi^2 = 0.049$ is obtained for $\lambda_c = 12722.8 \pm 0.2 \text{ \AA}$ and $\sigma = 106.2 \pm 11.9 \text{ km s}^{-2}$. Although the values obtained for λ_c and σ from Gauss-Hermite and Gaussian functions are similar, Fig. 2 clearly shows that the observed profile is better reproduced by Gauss-Hermite series than by a Gaussian curve – the blue wing present on the observed profile is not reproduced by the Gaussian curve. This conclusion is also evidenced by the lower χ^2 value obtained for the Gauss-Hermite fitting. In the other hand, the resulting χ^2 obtained for the fitting of the [Fe II] emission-line profile by two Gaussian curves $\chi_{2G}^2 = 0.011$ is similar to those obtained from the Gauss-Hermite fitting. However, in an automated fitting routine it is hard to decide when an emission-line profile should be fitted by a single Gaussian and when it should be fitted by multiple Gaussian curves (e.g. Storchi-Bergmann et al. 2010), while for Gauss-Hermite series this decision is done simple by varying the h_3 and h_4 moments.

In Riffel & Storchi-Bergmann (2010) we used PROFIT to study the gaseous kinematics of the inner $700 \times 700 \text{ pc}^2$ of Mrk 1066 using Gemini NIFS observations. The profiles of [P II] $\lambda 1.1886 \mu\text{m}$, [Fe II] $\lambda 1.2570 \mu\text{m}$, Pa β and H $_2$ $\lambda 2.1218 \mu\text{m}$ emission lines were fitted by Gauss-Hermite series in order to obtain the centroid velocity

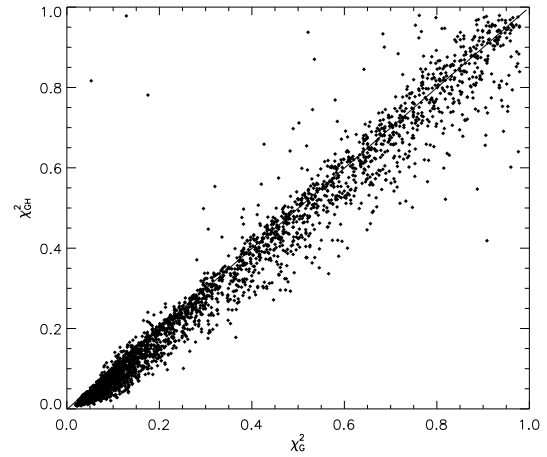


Fig. 3 Comparison of the resulting χ^2 obtained from the fitting of Gauss-Hermite series (y-axis) and Gaussian curves (x-axis) to the [Fe II] $\lambda 1.2570 \mu\text{m}$ emission-line profile of ~ 1800 spectra of the inner $700 \times 700 \text{ pc}^2$ of Mrk 1066.

field, velocity dispersion map and h_3 and h_4 maps for each emission line. The same observations presented in Riffel & Storchi-Bergmann (2010) were used to fit the [Fe II] $\lambda 1.2570 \mu\text{m}$ by Gaussian curves in order to compare the resulting fit with the ones obtained using Gauss-Hermite series. Figure 3 presents the comparison of the χ^2 values from the Gauss-Hermite fitting (χ_{GH}^2 – y-axis) with the ones obtained for the fitting of Gaussian curves (χ_G^2 – x-axis) for ~ 1800 spectra of the inner $700 \times 700 \text{ pc}^2$ of Mrk 1066 extracted within apertures of $0.05 \times 0.05 \text{ arcsec}^2$. As observed in this figure, χ_{GH}^2 is smaller than χ_G^2 for most spectra, indicating that the [Fe II] line profile in the central region of Mrk 1066 is better reproduced by Gauss-Hermite series than by Gaussian curves. A similar behavior is observed for [P II], H $_2$ and H emission lines at the same spatial region.

In order to illustrate the importance of properly map the emission line profile wings Fig. 4 presents a map for the h_3 Gauss-Hermite moment obtained for the Pa β emission in the central region of Mrk 1066. This map is similar to the ones obtained for the [Fe II] and [P II] emission lines (Riffel & Storchi-Bergmann 2010), showing several regions with values different than zero, indicating that the Pa β emission-line profile presents asymmetric deviation from a Gaussian curve, such as blue (negative values) and red (positive values) wings. In case of Gaussian fitting this information could be lost! The smallest values of up to -0.3 are observed at $\approx 1''$ north-west of the nucleus in a regions close to the edge of the radio structure (thick black contours). Some high values are also observed near to the edge of the radio jet to south-east of the nucleus. The presence of

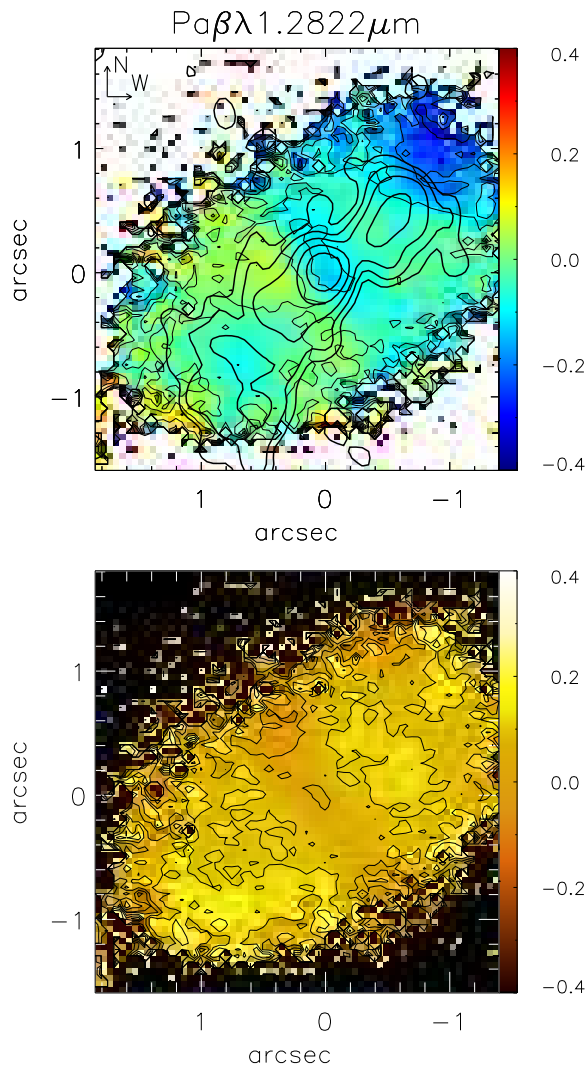


Fig. 4 Top: h_3 Gauss-Hermite moment map for $\text{Pa}\beta$ emission line on the inner $700 \times 700 \text{ pc}^2$ of Mrk 1066. The thick black contours are from the radio continuum emission of Nagar et al. (1999). Bottom: h_4 Gauss-Hermite moment map.

wings have also been observed by Knop et al. (2001) for the near-IR emission lines using long slit spectroscopy along the $\text{PA}=135^\circ$. These wings may be originated in an outflowing gas component driven by the radio jet, with the north-west side slightly oriented towards us and the south-east side away from us, being partially hidden by the disc of the galaxy. This interpretation is supported by the near-IR emission line kinematic maps, which show that the near-IR emitting gas presents at least three kinematics components: a rotating disk, an inflowing gas component and an outflowing component (Riffel & Storchi-Bergmann 2010). The above interpretation is also in good agreement with optical observations of the $[\text{O III}]$ emission, which seems to be originating in a bi-cone oriented along the same position angle $\text{PA} \approx 135^\circ$ – approximately the same orientation of the radio jet (Bower et al. 1995).

The h_4 map, shown in the bottom panel of Fig. 4, presents values near to zero in most locations of the central region of Mrk 1066. However, some positive h_4 -values are observed co-spatially with regions of lower velocity dispersion, indicating that part of the $\text{Pa}\beta$ emission originates from a colder gas than those which produces most of the line emission. For more details on the gaseous kinematics of the inner 350 pc radius of Mrk 1066 see Riffel & Storchi-Bergmann (2010).

5 Final Remarks

I presented a new routine to fit emission-line profiles from fits data cubes using Gauss-Hermite series or Gaussian curves, which provides a new alternative to the study of the emission-line flux distribution and kinematics for several astronomical objects. The PROFIT routine is written in IDL and is available at <http://www.ufsm.br/rogemar/software.html>. The main advantages of PROFIT compared with previous methods are:

- It allows the fitting of the line profiles by Gauss-Hermite series as an alternative to the ‘traditional’ Gaussian curves used in most studies and thus better describe the kinematics of the emitting gas.
- It is automated and can be applied directly on the final data cubes fits files from observations using most integral field units and Fabry-Perot interferometers.

A first application has been discussed for the case of near-IR emission-line profiles from the inner 350 pc of the Seyfert galaxy Mrk 1066. The main scientific conclusions are:

- The near-IR emission line profiles for this galaxy are better reproduced by Gauss-Hermite series than by

Gaussian curves, as indicated by the smaller χ^2 obtained for the former.

- The two-dimensional map for the h_3 Gauss-Hermite shows that the near-IR emission lines present asymmetric profiles, which can be explained as being originated in an outflowing gas driven by the radio jet.

Acknowledgments

I thank the referee for valuable suggestions which helped to improve the present paper. Based on observations obtained at the Gemini Observatory, which is operated by the Association of Universities for Research in Astronomy, Inc., under a cooperative agreement with the NSF on behalf of the Gemini partnership: the National Science Foundation (United States), the Science and Technology Facilities Council (United Kingdom), the National Research Council (Canada), CONICYT (Chile), the Australian Research Council (Australia), Ministério da Ciência e Tecnologia (Brazil) and Ministerio de Ciencia, Tecnología e Innovación Productiva (Argentina).

References

- Barbosa, C. L., Blum, R. D., Conti, P. S., Daminieli, A., Figuerêdo, E., 2008, *Astrophys. J.*, 678, 55.
- Barbosa, F. K. B., Storchi-Bergmann, T., Cid Fernandes, R., Winge, C., Schmitt, H., 2009, *Mon. Not. R. Astron. Soc.*, 396, 2.
- Beck, T. L., McGregor, P. J., Takami, M. & Pyo, T., 2008, *Astrophys. J.*, 676, 472.
- Blum, R. D. & McGregor, Peter J., 2009, *Astron. J.*, 138, 489.
- Bower, G., Wilson, A., Morse, J. A., Gelderman, R., Whittle, M., & Mulchaey, J., 1995, *Astrophys. J.*, 454, 106.
- Cappellari, M., Emsellem, E. 2004, *Publ. Astron. Soc. Pac.*, 116, 138.
- Davies, R. I.; Sánchez, F. M., Genzel, R., Tacconi, L. J., Hicks, E. K. S., Friedrich, S., Sternberg, A., 2007, *Astrophys. J.*, 671, 1388.
- Davies, R. I., Maciejewski, W., Hicks, E. K. S., Tacconi, L. J., Genzel, R., Engel, H., 2009, *Astrophys. J.*, 702, 114.
- Díaz, R. J., Dottori, H., Aguero, M. P., Mediavilla, E., Rodríguez, I., Mast, D., 2006, *Astrophys. J.*, 652, 1122.
- Emsellem, E. et al., 2007, *Mon. Not. R. Astron. Soc.*, 379, 401.
- Fathi, K., Storchi-Bergmann, T., Riffel, R. A., Winge, C., Axon, D. J., Robinson, A., Capetti, A., & Marconi, A., 2006, *Astrophys. J. Lett.*, 641, L25.
- Gerhard, O. E., 1993, *Mon. Not. R. Astron. Soc.*, 265, 213.
- Komossa, S., Xu, D., Zhou, H., Storchi-Bergmann, T. & Binette, L., 2008, *Astrophys. J.*, 680, 926.
- Hicks, E. K. S., Davies, R. I., Malkan, M. A., Genzel, R., Tacconi, L. J., Sánchez, F. M., Sternberg, A., 2009, *Astrophys. J.*, 696, 448.
- Knop, R. A., Armus, L., Matthews, K., Murphy, T. W., & Soifer, B. T., 2001, *Astrophys. J.*, 122, 764.
- McGregor, P., Dopita, M., Sutherland, R., Beck, T. & Storchi-Bergmann, T., 2007, *Astrophys. Space Sci.*, 311, 223.
- Moré, J. J., Garbow, B. S., & Hillstrom K. E., 1980, *User Guide for MINPACK1* (Argonne Nat. Lab. Rep. ANL8074; Argonne: Argonne National Laboratory).
- Nagar, N. M., Wilson, A. S., Mulchaey, J. S. & Gallimore, J. F., 1999, *Astrophys. J. Suppl. Ser.*, 120, 209.
- Peletier, R. F. et al., 2007, *New Astronomy*, 51, 29.
- Rodrigues, I., Dottori, H., Díaz, R. J., Agüero, M., P., Mast, D., 2009, *AJ*, 137, 4083.
- Riffel, Rogemar A., Storchi-Bergmann, T., Winge, C., Barbosa, F. K. B., 2006, *Mon. Not. R. Astron. Soc.*, 373, 2.
- Riffel, Rogemar A., Storchi-Bergmann, T., Winge, C., McGregor, P. J., Beck, T., Schmitt, H. 2008, *Mon. Not. R. Astron. Soc.*, 385, 1129.
- Riffel, Rogemar A., Storchi-Bergmann, T., Dors, O. L., Winge, C., 2009, *Mon. Not. R. Astron. Soc.*, 393, 783.
- Riffel, Rogemar A., Storchi-Bergmann, T., McGregor, P. J., 2009, *Astrophys. J.*, 698, 1767.
- Riffel, Rogemar A., Storchi-Bergmann, T., & Nagar, N. M., 2010, accepted by *Mon. Not. R. Astron. Soc.*
- Riffel, Rogemar A. & Storchi-Bergmann, T., 2010, submitted to *Mon. Not. R. Astron. Soc.*
- Sarzi, M. et al., 2006, *Mon. Not. R. Astron. Soc.*, 366, 1151.
- Steiner, J. E., Menezes, R. B., Ricci, T. V., Oliveira, A. S., 2009, *Mon. Not. R. Astron. Soc.*, 395, 64.
- Storchi-Bergmann, T., Dors Jr., O., Riffel, R. A., Fathi, K., Axon, D. J., & Robinson, A., 2007, *Astrophys. J.*, x, x.
- Storchi-Bergmann, T., McGregor, P. Riffel, Rogemar A., Simões Lopes, R., Beck, T., Dopita, M., 2009, *Mon. Not. R. Astron. Soc.*, 394, 1148.
- Storchi-Bergmann, T., Simões Lopes, R., McGregor, P. Riffel, Rogemar A., Beck, T., Dopita, M., 2010, *Mon. Not. R. Astron. Soc.*, tmp1898S, arxiv.org/abs/0911.2212.
- Takami, M., Beck, T. L., Pyo, T., McGregor, P., & Davis, C., 2007, *Astrophys. J.*, 670, 37.
- van der Marel, R.P. & Franx, M. 1993, *Astrophys. J.*, 407, 525